

Inhomogenous Primordial Baryon Distributions on Sub-Galactic Scales: High- z Galaxy Formation with WDM

Jesper Sommer-Larsen^{*}, Pavel Naselsky, Igor Novikov and Martin Götz

Theoretical Astrophysics Center, Juliane Maries Vej 30, 2100 Copenhagen, Denmark

Accepted —. Received —; in original form 2003 September 11

ABSTRACT

For the Warm Dark Matter (WDM) cosmological model the implications of strongly inhomogenous, primordial baryon distribution on sub-galactic scales for Big Bang Nucleosynthesis, Cosmic Microwave Background anisotropies and Galaxy Formation (including fully non-linear evolution to $z=0$) are discussed, and the inflationary theory leading to such distributions is briefly reviewed. It is found that Big Bang Nucleosynthesis is essentially unaffected relative to SBBN and that the change in recombination history at $z \sim 1500 - 700$ relative to “standard” theory leads to differences in the anisotropy and polarization power spectra, which should be detectable by the Planck satellite provided systematic effects can be accounted for. Moreover, it is shown by fully cosmological, hydro/gravity simulations that the formation of galactic discs is only weakly affected by going from smooth to highly non-homogenous, initial baryon distributions. In particular, the final disc angular momenta at $z=0$ are as large as for the standard case and the “disc angular momentum problem” is solved to within a factor of two or better without invoking (hypothetical) energetic feedback events. A very desirable difference relative to the the standard WDM model, however, is that the on-set of star (and AGN) formation happens earlier. For the “optimal” free-streaming mass scale of $M_f \sim 1.5 \cdot 10^{11} h^{-1} M_\odot$ the redshift of formation of the first stars increases from $z_{*,i}=4-5$ to $\gtrsim 6.5$, in much better agreement with observational data on high-redshift galaxies and QSOs. It will, however, not be possible to push $z_{*,i}$ above ≈ 10 , because at higher redshifts the gas velocity field is nowhere compressive. Probing the “dark ages” will hence enable a direct test of this theory.

Key words: galaxies: formation — cosmology: theory — cosmology: dark matter — cosmic microwave background

1 INTRODUCTION

One of the most intriguing challenges in modern cosmology is determining the origin and properties of the dark matter in the Universe. Progress can be made either through attempts to detect dark matter (elementary particles, massive compact halo objects (MACHOs), primordial black holes etc.) or indirectly by studying the implications of various dark matter candidates for the formation of galaxies, clusters of galaxies and the large-scale structure. The former approach has so far not given any definite results (except for the possible detection of micro-lensing by $\sim 0.5M_\odot$ MACHOs in the Galactic halo), so one is currently left with the latter.

The salient feature about “conventional” cold dark matter (CDM) is that as long as the dark matter particles are much heavier than 1 keV, the actual particle mass does not

matter for structure formation (assuming that the dark matter is elementary particles — note though, that axions, despite being ultra-light, behave like CDM). Structure formation in the CDM scenario faces a number of well known problems on galactic scales: 1) the steep central cusps problem (e.g. Moore et al. 1999b), 2) the angular momentum problem (e.g. Sommer-Larsen, Götz & Portinari 2003), 3) the missing satellites problem (e.g. Klypin et al. 1999) and possibly 4) the disc heating problem (e.g. Moore et al. 1999a). Going to the warm dark matter (WDM) structure formation scenario can considerably improve on problems 2-4 and possibly also on problem 1. On much larger scales, the scarcity of galaxies in voids could be a potential problem for CDM (Peebles 2001), which also may be remedied by going to WDM (Bode, Ostriker & Turok 2001).

The WDM structure formation scenario has, however, also at least one major problem in that it is difficult to get early enough galaxy formation to match observational constraints from high- z galaxies and QSOs. For a free-

^{*} E-mail: jslarsen@tac.dk

streaming mass scale of $M_f \sim 1.5 \cdot 10^{11} h^{-1} M_\odot$, which Sommer-Larsen & Dolgov (2001) found was the optimal value for solving the angular momentum problem, the first star formation takes place at $z \lesssim 6$ (see section 5). In contrast, both galaxies and QSOs have now been observationally detected at $z > 6$ (e.g., Hu et al. 2002, Fan et al. 2001) and the recent WMAP results possibly indicate that the reionization of the Universe took place at $z_{\text{re}} \gtrsim 10$ (Spergel et al. 2003).

The implicit assumption in standard WDM galaxy formation simulations is that at early times the baryons and the dark matter are distributed in the same way. The possibility exists, however, that the baryons could have a strongly inhomogeneous initial (primordial) density distribution. If on the (small) scale of these “baryon” clouds the fluctuations in the total matter density (baryons, dark matter and radiation, including neutrinos) are isocurvature fluctuations then the baryon clouds will not be smoothed out by Silk damping, nor will they suffer growth by gravitational instability any faster than the fluctuations in the dark matter density (Naselsky & Novikov 2002). Because of the higher gas density in the baryon clouds, the clouds will however cool out and form stars earlier than is the case in standard WDM simulations. The purpose of this paper is to quantify the effects of such initially inhomogeneous baryon distributions on the epoch of first star/galaxy formation as well as the subsequent disc formation. We also calculate how Big Bang Nucleosynthesis (BBN) and Cosmic Microwave Radiation Background (CMB) anisotropies are affected by going to this scenario, which we shall denote the WDMB model in the following.

In section 2 we describe the mix between adiabatic and isocurvature perturbations in the WDMB model, in section 3 inflationary models leading to such initial baryon clouds and in section 4 the resulting BBN and CMB anisotropy and polarization for the WDMB model. In section 5 we present our fully cosmological, hydro/gravity disc galaxy formation simulations, and finally, in section 6, we summarize our conclusions.

2 THE MIX BETWEEN ADIABATIC AND ISOCURVATURE PERTURBATIONS IN THE WDMB MODEL

In the framework of modern theories of inflation there are a lot of possibilities for having a mix of perturbation modes in the composite fluid, which are discussed by Riazuelo & Langlos (2000), Bartolo, Matarrese & Riotto (2001), Polarski & Starobinsky (1994), Abramo & Finelli (2001), Bucher, Moodley & Turok (2001) and others. The general idea for classifying modes of perturbations is based on a simple definition of the isocurvature modes. They do not perturb the gravitational potential meaning that the initial fluctuations of the total matter density ρ_{tot} are zero. In terms of the total density perturbation $\delta\rho_{\text{tot}}$ this corresponds to

$$\delta\rho_{\text{tot}} = \sum_{i=0}^N \rho_i \delta_i + 4\rho_\gamma(1 + R_{\nu\gamma}) \frac{\delta T}{T} = 0, \quad (1)$$

where ρ_i denotes the density of each massive species including baryons and different kinds of CDM and WDM particles, $\delta_i = \delta\rho_i/\rho_i$ is the density contrast for each massive component, $R_{\nu\gamma}$ is the density ratio between neutrinos ρ_ν and black body radiation ρ_γ , and $\delta T/T$ are the CMB temperature perturbations.

Using Eq. (1) one can find a certain peculiar mode (or modes) which compensates the contribution of baryonic perturbations to $\delta\rho_{\text{tot}}$, i.e. it corresponds to the condition $\rho_b \delta_b = -\rho_{dm} \delta_{dm}$ (we assume here without loss of generality that there is just one main dark matter component). We will denote this mode a compensating isocurvature mode (CIM) for the dark matter (Naselsky & Novikov 2002). As one can see this mode corresponds to $\delta T/T = 0$. This means that the CIM are equivalent to an isothermality perturbation. Note that exactly the same mode was described by Abramo & Finelli (2001), but for compensation between quintessence scalar field perturbations and some of the CDM particles.

The new aspect in the evolution of the isocurvature perturbations comes from the WDM model. If the rest mass of the dark matter particle is comparable to $m_x \simeq 1$ keV, then practically all perturbations at spatial scales smaller than the free streaming scale $\lambda_{\text{fs}} \simeq 0.2 \left(\frac{g_{\text{WDM,dec}}}{100}\right)^{-1/3} \left(\frac{m_x}{\text{keV}}\right)^{-1}$ Mpc are damped while at scales above λ_{fs} they behave like in the CDM model. The corresponding free-streaming mass in terms of the scale λ_{fs} is (Sommer-Larsen & Dolgov 2001)

$$M_{\text{fs}} = 3.7 \cdot 10^{11} \Omega_{\text{WDM}} h^{-1} \left(\frac{\lambda_{\text{fs}}}{0.1 h^{-1} \text{Mpc}}\right)^3 M_\odot \quad (2)$$

where $h = H_0/(100\text{km/s/Mpc})$ is the Hubble constant, $g_{\text{WDM,dec}}$ is the effective number of particle degrees of freedom when the WDM particle(s) decouple from the cosmic plasma, and

$$\Omega_{\text{WDM}} h^2 = \left(\frac{g_{\text{WDM,dec}}}{100}\right)^{-1} \left(\frac{m_x}{\text{keV}}\right). \quad (3)$$

This means that for pure adiabatic initial perturbations in the WDM model all inhomogeneities at the scales $M \leq M_{\text{fs}}$ are damped and baryons and WDM particles follow an approximately homogeneous and isotropic spatial distribution.

The situation changes dramatically if we instead of pure adiabatic perturbations have a mix between adiabatic and isocurvature modes of fluctuation. Let us discuss a model with isocurvature baryonic perturbations which have a typical spatial scale $\lambda \ll \lambda_{\text{fs}}$, but the corresponding amplitudes of perturbation are much higher than for the adiabatic tail of perturbations. This model is close to the baryon isocurvature fluctuations model (Dolgov & Silk 1993) and manifests itself as a combination of an adiabatic WDM model plus small-scale baryonic clouds. We shall denote this model the WDMB model.

Although we will consider in the non-linear galaxy formation calculations (Section 5) a strongly inhomogeneous, initial baryon density field + CIM, within the framework of isocurvature modes even if the condition $\rho_b \delta_b = -\rho_{dm} \delta_{dm}$ is *not* satisfied (e.g., with initially strongly non-homogeneous baryon + smooth dark matter density fields) the baryon density field will neither be smoothed out due to Silk damping, nor grow non-linear much before the dark matter density field due to gravitational instability (e.g.

Naselsky & Novikov 2002). We note, however, that for baryon “cloud” masses $M_{\text{cl}} \lesssim M_{\text{diff}} \simeq 10\text{--}20 M_{\odot}$ the baryon density field will be smoothed before the epoch of recombination due to baryon diffusion (Zeldovich & Novikov 1983).

Finally we note that Demianski & Doroshkevich (2003) recently also argued for small scale peculiarities in the power spectrum, albeit on other grounds.

3 BARYONIC CLOUDS AS A RELIC OF THE BARYOGENESIS EPOCH

It is necessary to note that the idea of a non-homogeneous distribution of baryonic matter at small scales is not new. The importance of entropy perturbations in the history of the cosmological expansion was *ad hoc* demonstrated by Doroshkevich, Zel’dovich & Novikov (1967) and Peebles (1967,1994) and recently generalized taking into account the multi-species structure of the cosmological plasma by Gnedin & Ostriker (1992), Hogan & Loeb (1993), Peebles & Juszkievich (1998). The possible inhomogeneities in the baryon distribution at the epoch of nucleosynthesis (Inhomogeneous Big Bang Nucleosynthesis (IBBS)) has been widely discussed in the literature (see the review by Jedamzik & Rehm 2001) in connection with the quark-hadron phase transition. But the typical scales of such inhomogeneities are extremely small compared to the typical mass scales of interest here - see below. Other events or processes have been suggested as possible sources of isocurvature perturbations partly connected with baryon re-distribution in space. For example, cosmic strings and corresponding currents and magnetic fields could generate specific features in baryonic matter distribution (Malaney & Butler 1989). Yokoyama & Sato (1991), Dolgov & Silk (1993), Polarski & Starobinsky (1994), Novikov, Schmalzing & Mukhanov (2000) have suggested various ways of generating isocurvature perturbations in the framework of inflation theory. Recently Naselsky & Novikov (2002) and Doroshkevich et al. (2003) have shown that baryonic clouds could mimic the acceleration of hydrogen recombination at redshift $z \simeq 10^3$ and produce corresponding peculiarities in the cosmic microwave background (CMB) anisotropy and polarization power spectrum.

Probably, the most interesting question in modern baryogenesis theory is how exactly the primordial soup of particle species became charge symmetry breaking and what the spatial distribution of the baryons might be. We will consider one of the most attractive models for baryonic cloud creation just after the end of inflation, suggested by Dolgov & Silk (1993) and similar to the Affeck & Dine (1985) baryogenesis model. We will assume that two scalar fields Φ and ϕ play as crucial a role in inflation as in charge symmetry breaking. Namely, that the field Φ determines the general properties of inflation while spontaneous CP violation is achieved by a condensate of the complex scalar field ϕ . Following Dolgov & Silk (1993), we will describe charge symmetry breaking using as the potential of the ϕ field

$$V(\phi) = m_{\text{eff}}^2 |\phi|^2 + \lambda |\phi|^4 \ln \left(\frac{|\phi|^2}{\sigma^2} \right), \quad (4)$$

where

$$m_{\text{eff}}^2 = -m_0^2 + \beta T^2 + \mu(\Phi - \Phi_{\text{cr}})^2 \quad (5)$$

is the effective mass of the ϕ field, including interaction with the inflaton Φ . m_0 is the vacuum mass of ϕ , Φ_{cr} the critical value of the Φ field when the effective mass m_{eff}^2 has a global minimum, and the βT^2 term corresponds to the temperature correction arising from the interaction of the ϕ field with the thermal bath, assuming no conformal coupling between ϕ and the curvature R . That all the constants m_0 , λ , μ , Φ_{cr} and β are assumed to be free parameters of the model allows us to optimize the resulting baryonic cloud properties.

Let us briefly describe some important stages in the Φ and ϕ field evolution during and right after the end of inflation. When inflation started, the initial value of the Φ field is assumed to be higher than the Planck mass, $\Phi_{\text{in}} > m_{\text{Pl}}$, and higher than Φ_{cr} as well, and $m_{\text{eff}}^2 > 0$. The potential $V(\phi)$ has a global minimum at $\phi = 0$ and roughly $V(\phi) \propto m_{\text{eff}}^2 |\phi|^2$. As one can see, the charge symmetry is unbroken. During the slow roll epoch of inflation the amplitude of the Φ field is a decreasing function of time, which is typical, for example, for the model of chaotic inflation, and when $\Phi = \Phi_{\text{cr}}$ the effective mass of the ϕ field reaches the minimum value $m_{\text{eff},\text{min}}^2 = -m_0^2 + \beta T^2 < 0$. The end of inflation corresponds to the condition $\Phi \simeq 0 \ll \Phi_{\text{cr}}$, while $m_{\text{eff}}^2 = -m_0^2 + \beta T^2 + \mu \Phi_{\text{cr}}^2 > 0$. Obviously, in the vicinity of the point $\Phi = \Phi_{\text{cr}}$ the effective mass $m_{\text{eff},\text{min}}^2$ can be negative, or positive but small, which means that it may happen that for some period of time $|m_{\text{eff},\text{min}}| < H_{\text{sr}}$, where H_{sr} is the value of the Hubble parameter during the slow roll decrease of the Φ field caused by inflation. Dolgov & Silk (1993) have shown that the phase transition of the ϕ field during the epoch $|m_{\text{eff},\text{min}}| < H_{\text{sr}}$ is essential for the formation of bubbles, which are governed by the quantum fluctuation of the ϕ field. The corresponding number density of the bubbles as a function of their mass M is (Dolgov & Silk 1993):

$$\frac{dn(M)}{dM} \simeq \frac{m_{\text{Pl}}^6}{M_0^4} \exp \left[-\alpha - \frac{\gamma}{4} \ln^2 \left(\frac{M}{M_0} \right) \right] \quad (6)$$

where

$$M_0 = \frac{1}{4} m_{\text{Pl}}^2 H_{\text{sr}}^{-1} \exp [2H_{\text{sr}}(t_e - t_{\text{cr}}) - 8\gamma^{-1}],$$

and $\alpha = \delta + 16\gamma^{-1}$, $\delta = \frac{4\pi^2 m_0^2}{3\lambda H_{\text{sr}}^2}$,

$$\gamma = \frac{4\pi^2 \mu}{3\lambda H_{\text{sr}}^4} \left(\frac{d\Phi}{dt} \right)^2 \Big|_{\Phi=\Phi_{\text{cr}}}.$$

t_e means the end of inflation and t_{cr} is the moment when $\Phi = \Phi_{\text{cr}}$. For the Φ field using slow roll approximation we obtain

$$\dot{\Phi} \simeq -\frac{1}{3H_{\text{sr}}} \frac{dV_{\text{in}}(\Phi)}{d\Phi}, \quad (7)$$

where $V_{\text{in}}(\Phi)$ is the inflaton potential. That lead to the following value for the γ parameter:

$$\gamma = \frac{4\pi^2 \mu}{27\lambda H_{\text{sr}}^6} \left(\frac{dV_{\text{in}}(\Phi)}{d\Phi} \right)^2 \Big|_{\Phi=\Phi_{\text{cr}}}. \quad (8)$$

As one can see from Eqs. (6) – (8), the distribution function $dn(M)/dM$ is strongly peaked at $M \sim M_0$, if the corresponding value of the γ parameter is $\gamma \gg 1$. In this case we can approximate $dn(M)/dM \propto \delta(M - M_0)$, where δ is the Dirac δ -function, and the corresponding mass M_0

is a function of the fundamental parameters, namely, H_{sr} , t_e and t_{cr} . Dolgov & Silk (1993) have shown that the simplest way to have a large value for the baryon asymmetry inside the bubbles is to assume that CP-nonconservation is proportional to the value of the scalar field ϕ which is much larger than that outside the clouds. Thus, because of bubble formation during inflation, and using CP-nonconserving effects, the baryonic matter can have some strong perturbation strongly peaked at some characteristic mass scale M_0 . It is not possible at present to calculate the value of M_0 from first principles, but we shall assume in the following that $M_{\text{diff}} \lesssim M_0 \ll M_{\text{fs}}$ (Section 2).

For simplicity we suppose that all baryonic clouds have the same characteristic size $R_{\text{cl}} \propto M_0^{1/3}$, which is much smaller than the size of the horizon R_{rec} at the epoch of recombination ($z \sim 10^3$), $R_{\text{cl}} \ll R_{\text{rec}}$. We denote by $\rho_{\text{b,in}}$ and $\rho_{\text{b,out}}$ the baryon density inside and outside the clouds. Then the mean density $\rho_{\text{b,mean}}$ at scales much greater than R_{cl} and distances between them, is

$$\rho_{\text{b,mean}} = \rho_{\text{b,in}}f + \rho_{\text{b,out}}(1 - f), \quad (9)$$

where f is the volume fraction of the clouds. We denote

$$\eta = \frac{\rho_{\text{b,in}}}{\rho_{\text{b,out}}}. \quad (10)$$

Using this one obtains the following relations between the mean value of the baryon density and its inner and outer values

$$\rho_{\text{b,in}} = \frac{\eta\rho_{\text{b,mean}}}{1 + f(\eta - 1)}, \quad (11)$$

and

$$\rho_{\text{b,out}} = \frac{\rho_{\text{b,mean}}}{1 + f(\eta - 1)}. \quad (12)$$

Using the quantities f and η we can define the baryonic mass fraction of the clouds

$$F_{\text{b}} = \frac{\eta f}{1 + f(\eta - 1)}. \quad (13)$$

Obviously, all the parameters f , η and F_{b} are the result of fine tuning the inflaton $V_{\text{in}}(\Phi)$ and ϕ scalar field potentials leading to the formation of the baryonic asymmetry in the Universe.

4 BARYONIC CLOUDS AND THEIR COSMOLOGICAL CONSEQUENCES

There are several sources of information on $\Omega_{\text{b}} = \rho_{\text{b}}/\rho_{\text{cr}}$, where ρ_{b} and ρ_{cr} are the present values of the baryonic and critical densities. One comes from the confrontation of the Standard Big Bang Nucleosynthesis (SBBN) theory with observational data (see the review by Fukugita, Hogan & Peebles 1998). The corresponding value of the baryonic density from this line of argument is $\Omega_{\text{b}}h^2 = 0.019 \pm 0.001$. An additional empirical relation between baryonic and total matter fractions $f_{\text{b}} = \Omega_{\text{b}}/\Omega_{\text{M}} \sim 0.1 - 0.15$ for $h = 0.7$ comes from X-ray data on clusters of galaxies (Carlberg et al. 1996; Ettori & Fabian 1999). For the most popular Λ CDM cosmological model with $\Omega_{\text{M}} \simeq 0.3$ and $\Omega_{\Lambda} \simeq 0.7$, the corresponding value of $\Omega_{\text{b}}h^2$ is ~ 0.02 , in agreement with the SBBN predictions (Mason et al. 2003).

An independent and important information about the

baryonic fraction in the Universe comes from recent CMB experiments such as BOOMERANG (de Bernardis et al. 2000), MAXIMA-1 (Hanany et al. 2000), CBI (Mason et al. 2003), and DASI (Leitch et al. 2002). Fitting the CMB anisotropy power spectrum to the above-mentioned observational data (Tegmark & Zaldarriaga 2000; White et al. 2000; Lesgourgues & Peloso 2000) indicates that the baryon fraction parameter should be significantly larger than the SBBN expected value, namely, $\Omega_{\text{b}}h^2 \simeq 0.03$. However, Bond & Crittenden (2001) showed that new BOOMERANG, MAXIMA-1 and DASI data do not contradict $\Omega_{\text{b}}h^2 = 0.022 \pm 0.004$.

It is worth noting that the above mentioned methods for the baryonic fraction density estimation from CMB and SBBN predictions are based on the simple idea that the distribution of matter (including dark matter particles and baryons) is nearly homogeneous on all scales, except for small fluctuations leading to galaxy and large-scale structure formation. Typically, these are assumed to be adiabatic. One can ask how sensitive conclusions based on the BBN + CMB data are to the presence of small-scale baryonic (non-linear) clouds before cosmological recombination.

4.1 Big Bang Nucleosynthesis (BBN)

In the framework of the SBBN model the baryonic fraction of matter and its spatial distribution play a crucial role starting from the epoch, when the balance between neutrinos ($\nu_e, \bar{\nu}_e$), neutrons (n) and protons (p) in reactions $n + \nu_e \leftrightarrow p + e^-$, $n + e^+ \leftrightarrow p + \bar{\nu}_e$, $n \rightarrow p + e^- + \bar{\nu}_e$ was broken. The corresponding time of violation of the neutrino-baryon equilibrium is close to $\tau_{\nu_e,p} \simeq 1$ sec when the temperature of the plasma was close to $T_{\nu_e,p} \simeq 10^{10} K$ (see the review by Olive, Steigman & Walker 2000). The time scale $\tau_{\nu_e,p}$ determines the characteristic length $l_{\nu_e,p} \simeq c\tau_{\nu_e,p}$, which in terms of the baryonic mass fraction of matter corresponds to

$$M_{\nu_e,p} \sim m_{\text{pl}} \left(\frac{\tau_{\nu_e,p}}{t_{\text{pl}}} \right) \left(\frac{\rho_{\text{b}}}{\rho_{\gamma}} \right) \Big|_{t=\tau_{\nu_e,p}} \simeq 3 \cdot 10^{-3} \left(\frac{\Omega_{\text{b}}h^2}{0.02} \right) M_{\odot}, \quad (14)$$

where t_{pl} is the Planck time, ρ_{b} and ρ_{γ} are the densities of baryons and radiation in the standard cosmological model without baryonic clouds. The light elements (chiefly, ${}^4\text{He}$ and deuterium) were completely synthesized by $\tau_{\text{end}} \sim 3 \cdot 10^2 - 10^3$ s. In terms of the baryonic mass scale it corresponds to

$$M_{\text{end}} \simeq M_{\nu_e,p} \left(\frac{\tau_{\text{end}}}{\tau_{\nu_e,p}} \right)^{3/2} \simeq 16 \left(\frac{\tau_{\text{end}}}{300\text{s}} \right)^{3/2} \left(\frac{\Omega_{\text{b}}h^2}{0.02} \right) M_{\odot}. \quad (15)$$

Thus, if the characteristic mass scale M_0 for the baryonic clouds is higher than M_{end} ($\sim M_{\text{diff}}$ cf. section 2), the cosmological nucleosynthesis in each cloud is independent of the others and the mean mass fraction of each chemical element is related with the mass fraction of the clouds as

$$\langle Y_k \rangle = \frac{1}{V} \int^{V_{\text{cl}}} d^3r \left(\frac{\rho_{\text{in}}(\vec{r})}{\rho_{\text{mean}}} \right) Y_k^{\text{in}}(\rho_{\text{in}}(\vec{r})) + \frac{1}{V} \int^{V - V_{\text{cl}}} d^3r \left(\frac{\rho_{\text{out}}(\vec{r})}{\rho_{\text{mean}}} \right) Y_k^{\text{out}}(\rho_{\text{out}}(\vec{r})) \quad (16)$$

where $V_{\text{cl}}/V = f$, V is the volume and Y_k^{in} , Y_k^{out} are the inner and outer mass fractions of the k th element. If we

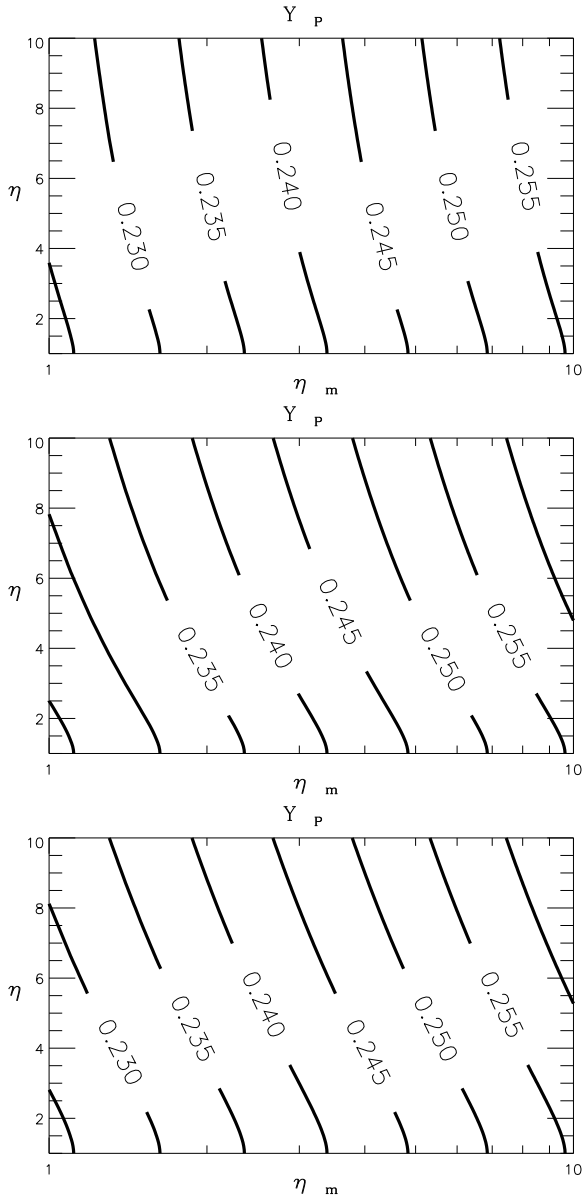


Figure 1. The mean mass fraction of ${}^4\text{He}$ as a function of η_m and η for different baryonic mass fractions F_b . From top to bottom $F_b = 0.2, 0.5, 0.8$.

assume that inside the clouds the density $\rho_{\text{in}}(\vec{r})$ is uniformly and isotropically distributed then from Eq. (11)–(13) and Eq. (16) we obtain

$$\langle Y_k \rangle = Y_k^{\text{in}}(\rho_{\text{in}})F_b + Y_k^{\text{out}}(\rho_{\text{out}})(1 - F_b) \quad (17)$$

In Fig. 1 and Fig. 2 we show the dependence of the mean fraction of ${}^4\text{He}$ and D on $\eta_m = 10^{10}\langle n_b \rangle / n_\gamma = 274\langle \Omega_b \rangle h^2$ and η for such a model. The three panels of Fig. 1 show different values of the mass fraction $F_b = 0.2$ (top), $F_b = 0.5$ (middle) and $F_b = 0.8$ (bottom). As one can see from Fig. 1, if the $\langle \Omega_b \rangle h^2$ parameter is close to $\langle \Omega_b \rangle h^2 = 0.022$ ($\eta_m \sim 5$), and $\eta = 1$, then the mean mass fraction of helium is equal to Y_p in the standard model (without clouds) and corresponds to $Y_p = 0.247$. For the model $F_b = 0.2$, $1 \leq \eta \leq 10$ and $\eta_m \sim 5$ the mean helium mass fraction lies in the range $0.247 \leq$

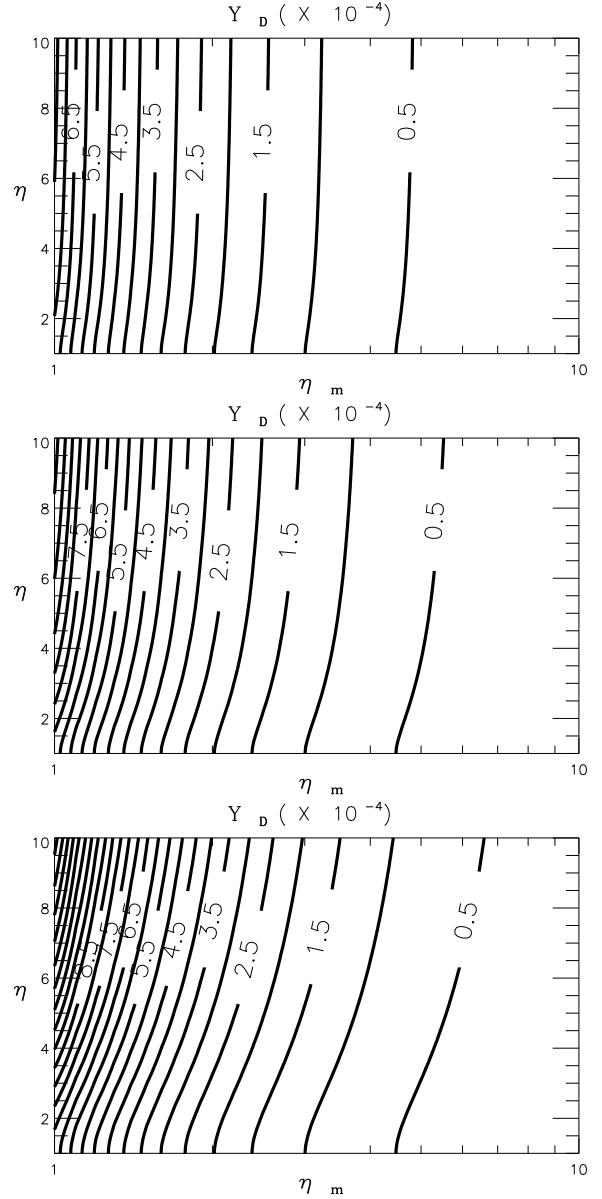


Figure 2. The mean mass fraction of D as a function of η_m and η and the same F_b parameters as in Fig. 1.

$\langle Y_p \rangle \leq 0.252$ which corresponds to the 2% relative deviation from the value $Y_p = 0.247$. For the model with $F_b = 0.5$, as it follows from Fig. 1, the maximum value of $\langle Y_p \rangle = 0.256$ is achieved for $\eta = 10$ and the corresponding deviation is 3%. For the model with $F_b = 0.8$ we obtain a quite similar result: $\langle Y_p \rangle \leq 0.256$ for all values in $\eta \leq 10$. Since the uncertainty in the observationally determined value of Y_p is $\sim 5\%$ (when systematics are included — B. Pagel 2003, private communication) then even if η_m was known to high precision (e.g. from the CMB data) it would not be possible to distinguish between the smooth and clumpy initial baryon distribution scenarios using BBN.

For the primordial mass fraction of deuterium the dependence of $\langle Y_D \rangle$ on η , η_m and F_b is shown in Fig. 2. As can be seen from the figure, for $\eta_m \sim 5$ and $\eta = 1$ the mass fraction of deuterium is close to $\langle Y_{D,\text{st}} \rangle \simeq 4 \cdot 10^{-5}$. Moreover,

for $\eta \leq 10$ and $F_b = 0.2, 0.5, 0.8$ the corresponding variation of $\langle Y_D \rangle$ is $\lesssim 20 - 30\%$ for $\eta_m \sim 5$. As this is less than the uncertainty on the observationally determined value of $\langle Y_D \rangle$ ($\sim 40\%$ - B. Pagel 2003, private communication) this can not be used either to select between the two classes of models.

For both ^4He and D, if η is increased beyond $\eta=10$ the further change in Y_p and Y_D for a given η_m is small compared to the above mentioned observational uncertainties.

4.2 CMB Anisotropy and Polarization

As was mentioned by Naselsky & Novikov (2002), the presence of the baryonic clouds in the primordial hydrogen-helium plasma at redshift $z \sim 10^3$ changes the dynamics of hydrogen recombination due to the non-linear dependence of the ionization fraction x_e on the baryon density. During the period of recombination diffusion of baryons from inner to outer regions of the clouds can suppress any small scale irregularities inside the clouds. The natural length scale of this process is of the order of the Jeans length $R_J \sim c_s t_{\text{rec}}$, where c_s is the baryonic sound speed and t_{rec} is the corresponding time when the plasma became transparent for the CMB radiation (Liu et al. 2001; Naselsky & Novikov 2002). For adiabatic perturbations at scales $M \gg 10^{13} M_\odot$ (which are the sources of the Doppler peaks in the CMB anisotropy and polarization power spectra) the evolution during the period of recombination depends not on the ionization fraction inside or outside the clouds, but rather on the mean value of the ionization fraction at the scales of adiabatic perturbations. This mean ionization fraction does not correspond to the ionization fraction for the mean value of the baryonic density due to non-linear effects.

For the cloudy baryonic model we introduce the mean value of the electron density

$$\langle n_e \rangle = n_{e,\text{in}} f + n_{e,\text{out}} (1 - f), \quad (18)$$

where $n_{e,\text{in}}$ and $n_{e,\text{out}}$ are the number densities of free electrons inside and outside the clouds and

$$\begin{aligned} n_{e,\text{in}} &= x_{e,\text{in}} (1 - Y_{\text{He},\text{in}}) n_{b,\text{in}}, \\ n_{e,\text{out}} &= x_{e,\text{out}} (1 - Y_{\text{He},\text{out}}) n_{b,\text{out}}, \end{aligned} \quad (19)$$

where $x_{e,\text{in}}$, $x_{e,\text{out}}$, $Y_{\text{He},\text{in}}$ and $Y_{\text{He},\text{out}}$ are the ionization fractions and helium mass fractions for the inner and outer regions, and the nucleon number density is denoted n_b . Note that by definition $x_e = n_e/n_H$, where n_H is the number density of neutral and ionized hydrogen. Let us introduce the mean value of the ionization fraction $\langle x_e \rangle$,

$$\langle x_e \rangle = \frac{\langle n_e \rangle}{\langle n_b \rangle} (1 - \langle Y_{\text{He}} \rangle)^{-1}, \quad (20)$$

then

$$\langle x_e \rangle = x_{e,\text{in}} G_{\text{in}} + x_{e,\text{out}} G_{\text{out}}, \quad (21)$$

where

$$\begin{aligned} G_{\text{in}} &= \frac{\xi f}{1 + f(\xi - 1)} \left(\frac{1 - Y_{p,\text{in}}}{1 - \langle Y_p \rangle} \right), \\ G_{\text{out}} &= \frac{1 - f}{1 + f(\xi - 1)} \left(\frac{1 - Y_{p,\text{out}}}{1 - \langle Y_p \rangle} \right), \end{aligned} \quad (22)$$

and $\langle Y_p \rangle$ denotes the mean mass fraction of helium.

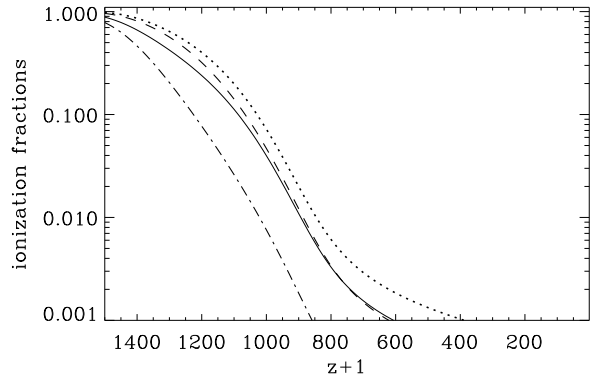


Figure 3. The rate of ionization for the clumpy baryonic model. The dash-dotted line corresponds to the ionization fraction for the inner regions. The dotted line is the ionization fraction for the outer regions. The solid line is the mean fraction of ionization. The dashed line is the ionization fraction for the model with $\Omega_b h^2 = 0.022$ without clouds.

In Fig. 3 we plot the functions $x_{e,\text{in}}$, $x_{e,\text{out}}$, and $\langle x_e \rangle$ for $\langle \Omega_b h^2 \rangle = 0.022$, $h = 0.7$, $\eta = 11$, and $f = 0.1$, and cosmological parameters $\Omega_K = 0$ (the curvature parameter), $\Omega_\Lambda = 0.7$ (vacuum density) and $\Omega_{\text{WDM}} h^2 = 0.125$ (WDM density). A modified version of the RECFAST code was used for the calculations.

As one can see from this figure the fractions of ionization $\langle x_e \rangle$, $x_{e,\text{in}}$ and $x_{e,\text{out}}$ have different shapes, and different asymptotic behaviours at “low redshifts”. In the range $700 \lesssim z \lesssim 1500$ recombination is somewhat accelerated and for $z \lesssim 700$ slightly delayed compared to “standard” recombination.

In order to compare the CMB anisotropy and polarization power spectrum in the cloudy baryonic model with the standard one (without clouds) we modify the CMBFAST code (Seljak & Zaldarriaga 1996), by taking into account the more complicated ionization history of the plasma. For the comparison we assume in both cases (late) full reionization corresponding to a value of the optical depth of $\tau_r = 0.1$. τ_r is related to the redshift of full reionization z_r as

$$\begin{aligned} z_r &= 13.6 \left(\frac{\tau_r}{0.1} \right)^{2/3} \left(\frac{1 - \langle Y_p \rangle}{0.76} \right)^{-2/3} \times \\ &\left(\frac{\langle \Omega_b h^2 \rangle}{0.022} \right)^{-2/3} \left(\frac{\Omega_{\text{WDM}} h^2}{0.125} \right)^{1/3}, \end{aligned} \quad (23)$$

so $\tau_r = 0.1$ corresponds to a redshift of reionization of $z_r \simeq 14$ (the following results do not change in any significant way if $\tau_r=0.05$ or 0.15 is adopted instead). In Fig. 4 we plot the CMB anisotropy power spectra for the standard and cloudy WDM models together with the latest BOOMERANG, MAXIMA-1, and CBI observational data (the very recent WMAP data are essentially in complete agreement with the above data, Spergel et al. 2003). As can be seen from the figure small deviations of the power spectrum appear, but both models are in agreement with the data of the CMB experiments (see also Table 1).

To illustrate the effect of baryonic clouds in the WDM model and to compare with the standard WDM model, taking into account the expected sensitivity of the PLANCK

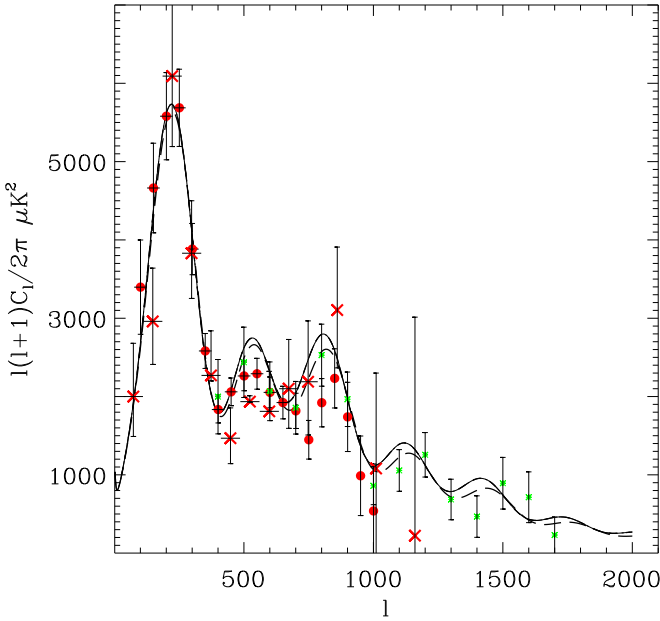


Figure 4. The CMB power spectra for the WDM models. The solid line corresponds to the standard model, the dashed line to the cloudy baryonic WDM model.

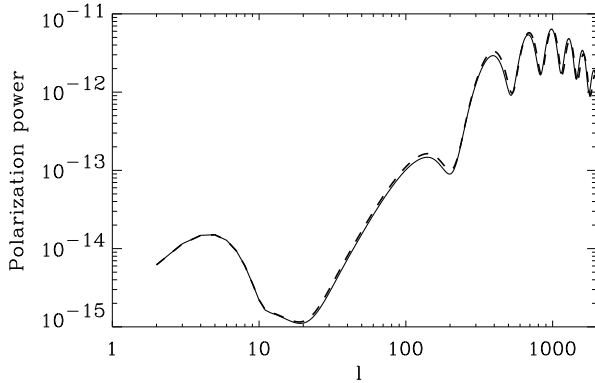


Figure 5. The CMB polarization power spectra for the WDM models. The solid line corresponds to the standard model, the dashed line to the cloudy baryonic WDM model.

experiment, we describe the deviations of the anisotropy and polarization power spectra in terms of the functions

$$\begin{aligned} D^a(l) &= 2 [C_b^a(l) - C_s^a(l)] / [C_b^a(l) + C_s^a(l)] , \\ D^p(l) &= 2 [C_b^p(l) - C_s^p(l)] / [C_b^p(l) + C_s^p(l)] , \end{aligned} \quad (24)$$

where $C_b^a(l)$ and $C_s^a(l)$ are the CMB anisotropy power spectra for the baryonic clouds and smooth baryon models, respectively, and $C_b^p(l)$ and $C_s^p(l)$ are the corresponding polarization power spectra. Obviously, it is necessary to compare the functions $D^a(l)$ and $D^p(l)$ with the errors of the $C(l)$ extraction for the PLANCK mission.

Assuming that systematic effects can be essentially removed, the uncertainty should be close to the cosmic variance limit

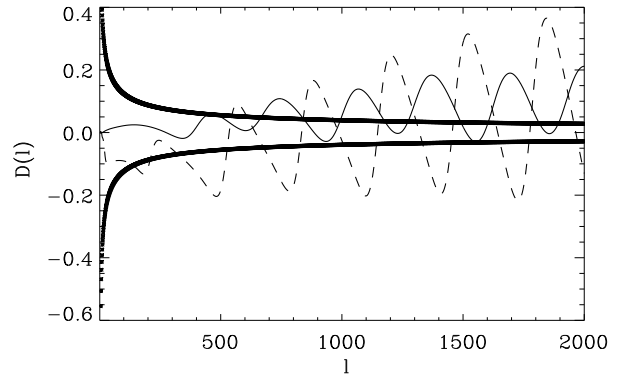


Figure 6. $D^a(l)$ and $D^p(l)$ for the CMB anisotropy and polarization power spectra in WDM models. The solid line corresponds to anisotropy, the dash line is the polarization. The thick solid line corresponds to the cosmic variance effect.

$$\frac{\Delta C(l)}{C(l)} \simeq \frac{1}{\sqrt{f_{\text{sky}}(l + \frac{1}{2})}} [1 + w^{-1} C^{-1}(l) W_l^{-2}] , \quad (25)$$

$$w = (\sigma_p \theta_{\text{FWHM}})^{-2}, \quad W_l \simeq \exp \left[-\frac{l(l+1)}{2l_s^2} \right], \quad f_{\text{sky}} \simeq 0.65 .$$

Here f_{sky} is the sky coverage during the first year of observations, σ_p is the sensitivity per resolution element $\theta_{\text{FWHM}} \times \theta_{\text{FWHM}}$ and $l_s = \sqrt{8 \ln 2} \theta_{\text{FWHM}}^{-1}$. In Fig. 6 we plot the functions $D^a(l)$ and $D^p(l)$ for $2 < l < 2000$ and show the uncertainty due to cosmic variance.

For example, for the HFI PLANCK 214 GHz channel θ_{FWHM} is 5.5 arcmin and the errors at $l \leq 2000$ are dominated by the first term in Eq. (25). As one can see from Fig. 6, at $l \sim 1000 - 1500$ the peak-to-peak amplitudes are $\sim 10 - 20\%$, while $\Delta C(l)/C(l) \simeq 5 - 7\%$. This means that such signals in the anisotropy power spectrum can be detected by the PLANCK mission, if the systematic effects can be accounted for to better than $\sim \Delta C(l)/C(l) \simeq [f_{\text{sky}}(l + 1/2)]^{-1/2}$.

As one can see from Fig. 6 the polarization power spectra are even more sensitive to distortions of the ionization history of the Universe in the WDM model with baryonic clouds. Recently the DASI experiment (Leitch et al. 2002) has detected CMB polarization without a significant presence of polarized foregrounds. This implies that the PLANCK mission potentially will be able to measure the polarization of the CMB with unprecedented accuracy, probably close to the cosmic variance limit, which means that peculiarities of the polarization power spectrum caused by baryonic clouds could be observationally detected, if present, during the coming years.

5 DISC GALAXY FORMATION WITH BARYONIC CLUMPS

The uneven distribution of baryons in this model could of course have consequences for the formation of disc galaxies. The baryonic clumps are additional structures, which would not be present in “normal” galaxy formation scenarios. They could possibly disturb the assembly of discs, similar to the

Table 1. CMB power spectrum χ^2 parameters for the WDM and WDMB models.

Obs/Mod	BOOM	MAXIMA	CBIM1	CBIM2	VSA
Dof	12	10	7	7	20
Standard model (WDM)	11.2	14.1	3.20	7.15	7.08
Cloudy model (WDMB)	8.69	11.3	1.60	5.62	6.59

angular momentum problem in CDM cosmologies (see, e.g., Navarro & Benz 1991, Navarro & White 1994, Navarro & Steinmetz 1997, Bryan 2002, Sommer-Larsen, Götz & Portinari 2003). For CDM, the early formation of small haloes leads to many merging events, during which the subclumps, which later form the central disc, can lose energy and orbital angular momentum by dynamical friction, resulting in discs with too little specific angular momentum. The presence of baryonic clumps may aggravate this problem, and may even effectively prevent the formation of galactic discs. To investigate this, we ran a series of TreeSPH simulations of galaxy formation, described in this section, with and without such clumps.

5.1 The Code

We use the gridless Lagrangian N-body and Smoothed Particle Hydrodynamics code TreeSPH described in Sommer-Larsen, Gelato & Vedel (1999), which is modelled after that of Hernquist & Katz (1989).

Radiative gas cooling is included in the simulations (Sutherland & Dopita 1993). Some are run with a primordial abundance cooling function, in which case radiative heating due to a metagalactic UV field is included. This homogeneous and isotropic, redshift-dependent UV background corresponds to the UV field produced by AGNs and young galaxies. It is modelled after Haardt & Madau (1996) and switches on at a redshift of $z = 6$. Its effects on the cooling function are included as discussed e.g. in Vedel, Hellsten & Sommer-Larsen (1994). Other simulations were run with an about 1/3 solar metallicity cooling function (more precisely with $[\text{Fe}/\text{H}] = -0.5$). This is the metal abundance of the intracluster medium and can probably be considered a reasonable upper limit to the metal abundance of disc forming gas. In this case, the metagalactic UV field is not included, since it does not play a major role because of the very high cooling efficiency due to the metals. Furthermore, all simulations incorporate inverse Compton cooling, which is also explicitly redshift-dependent.

For the gas dynamics, the smoothing length of each SPH particle is adjusted to keep the number of neighbors close to 50, and the shear-free Balsara viscosity (Balsara 1995) is used, instead of the standard Monaghan-Gingold viscosity (Monaghan & Gingold 1983).

5.2 The Star Formation Recipe

Star formation is accounted for by converting SPH particles into star particles, keeping the total number of these particles constant. We assume that star formation sets in when the hydrogen number density exceeds a threshold of $n_{\text{H},c} = 0.01 \text{ cm}^{-3}$. This may seem quite low, but is still large enough

to ensure that the gas has cooled below a critical temperature of $T \sim 10^4 \text{ K}$, at which the radiative cooling function is effectively truncated. In addition to the density criterion, the divergence of the velocity field has to be negative in the star forming region. As will be seen later, this second condition is very important for simulations with WDMB.

Star formation occurs then on a time scale

$$t_* = \frac{t_{\text{dyn}}}{\varepsilon} = \frac{1}{\sqrt{4\pi G \rho_{\text{gas}}}} \frac{1}{\varepsilon},$$

governed by the dynamical time scale t_{dyn} and a star formation efficiency (SFE) ε . The SFE is quite small in the Galactic disc at present, at most a few percent (e.g. Silk 1997). Therefore, most simulations are run with a SFE $\varepsilon = 0.01$. But to account for the possibility of more efficient star formation in the early universe, we also use $\varepsilon = 0.1$ and $\varepsilon = 1$ for some of the simulations. As is customary, the actual point in time, when a SPH particle is converted to a star particle, is then determined probabilistically, based upon its star formation time scale.

The SFE is kept constant in time, which is of course unrealistic for the cases with high SFE $\varepsilon = 0.1$ and $\varepsilon = 1$. The high-SFE simulations were primarily run to see what effect the SFE has on the onset of star formation at high redshifts.

Feedback is not included in the simulations. Even though it may be important in the early stages of galaxy formation (e.g. Sommer-Larsen, Götz & Portinari 2003), it is probably not at later times. In the warm dark matter (WDM) cosmological scenario, which is used here (see below), the angular momentum problem, as well as other problems on galactic scales related to CDM, can be significantly reduced without invoking feedback (Sommer-Larsen & Dolgov 2001). In any case, the absence of feedback in the simulations can be regarded as a conservative approach, since its inclusion would possibly result in even more realistic galactic discs (Sommer-Larsen, Götz & Portinari 2003).

5.3 Cosmological Parameters and Initial Conditions

The cosmological initial conditions are based on a flat Λ WDM model with $\Omega_M = 0.3$ and $\Omega_\Lambda = 0.7$. The Hubble parameter is chosen to be $H_0 = 100h \text{ km/s/Mpc} = 65 \text{ km/s/Mpc}$, yielding a present age of the universe of 14.5 Gyr. The initial power spectrum of density fluctuations is cluster abundance normalized to give a $\sigma_8 = 1.0$ at $z=0$ (Eke, Cole & Frenk 1996 — adopting $\sigma_8 = 0.9$ does not lead to any significant changes of the results presented in the following). For the WDM particle, we use a free-streaming mass of $1.5 \cdot 10^{11} h^{-1} M_\odot$, corresponding to

Table 2. Physical properties of the two selected disc galaxies in the different simulation runs. A ‘0’ in the column ‘# of clumps’ means that the simulation was run with evenly distributed baryonic matter, otherwise the number of clumps in the initial galaxy forming region is given. [Fe/H] is the metallicity, with ‘prim.’ denoting the primordial value, ε the star formation efficiency, M_* and M_{cg} the masses in stars and cold gas ($T < 3 \cdot 10^4$ K), respectively, V_c the circular velocity, j_{tot} the specific angular momentum of the disc, including stars and cold gas, and j_* the specific angular momentum of the stars only. The quantities in the last five columns are for within 40 kpc of the center of the disc.

Galaxy	# of clumps	[Fe/H]	ε	M_* [$10^{10} M_\odot$]	M_{cg} [$10^{10} M_\odot$]	V_c [km / s]	j_{tot} [kpc · km / s]	j_* [kpc · km / s]
19	0	prim.	0.01	4.97	0.83	209	511	341
19	0	-0.5	0.01	6.98	1.81	218	1433	961
19	248	prim.	0.01	5.41	0.76	213	557	422
19	248	prim.	0.1	4.64	0.05	195	271	270
19	248	prim.	1.0	4.35	0.004	185	292	292
19	248	-0.5	0.01	7.98	1.27	229	1119	878
27	0	prim.	0.01	3.50	0.53	179	466	224
27	0	-0.5	0.01	5.17	1.01	196	934	493
27	177	prim.	0.01	3.65	0.62	182	536	331
27	177	prim.	0.1	3.70	0.27	178	458	336
27	177	prim.	1.0	3.34	0.09	161	432	404
27	177	-0.5	0.01	6.31	1.13	217	851	621

a free-streaming scale of $0.11h^{-1}$ Mpc and a WDM particle mass of $1.2h^{5/4}$ keV. These numbers are consistent with the values used by Sommer-Larsen & Dolgov (2001) for solving (to within a factor of two) the angular momentum problem with WDM. In addition, the same sharp cut-off of the WDM power spectrum below the free-streaming scale is used here.

In order to select interesting candidate galaxies for further study, we ran at first a dark matter-only N-body simulation in a $10h^{-1}$ Mpc box with 128^3 particles, using the Hydra code (Couchman, Thomas & Pearce 1995) and starting at an initial redshift $z_{\text{ini}} = 19$. The usual set-up, where particles are displaced from a regularly spaced grid, can not be used in WDM simulations, as this leads to the formation of spurious low-mass haloes evenly spaced along the forming filaments, which are non-physical artifacts. (See Götz & Sommer-Larsen 2002 for a detailed discussion.) We therefore start from glass-like initial conditions (White 1996) where the particles are irregularly distributed, but still (almost) evenly spaced.

At redshift $z = 0$, haloes in the pure dark matter simulation are identified with a friends-of-friends algorithm, where gravitationally unbound particles are removed. The galaxies then selected for detailed simulation with the TreeSPH code had to be sufficiently isolated (at least 1 Mpc away from galaxy groups and 0.5 Mpc away from larger galaxies at $z = 0$) and had not to undergo a major merger (with mass ratio more than 1:3) since $z = 1$.

To simulate the formation of the selected galaxies, baryonic matter has to be added to the initial conditions. We aimed at obtaining a baryonic fraction $f_b \approx 0.1$, consistent with nucleosynthesis constraints and with observed baryonic fractions in groups and clusters (see e.g. Ettori & Fabian (1999)). Our choice of f_b is a bit low compared to recent estimates of Ω_b and Ω_M (section 4), but this has no consequences for any of the following results.

For the simulations with baryonic clumps, we choose the most extreme situation where all of the baryonic matter

is initially contained inside spherical clumps, whereas the dark matter is exclusively found outside of them. That way, we maximize the effect, which the clumps have on galaxy formation. The easiest way to achieve the desired baryonic fraction $f_b \approx 0.1$ is then to remove 10% of the original 128^3 dark matter particles from spherical subregions of the cosmological simulation, and fill these regions with gas particles. To get (approximately) the same number of particles as in the simulations, where the baryonic matter is distributed evenly, we use 128^3 SPH particles for that purpose, such that each has a mass f_b times that of a dark matter particle. We therefore get in the clumps a $10\times$ higher resolution (in terms of particle number density) than in the surroundings, where only dark matter is found, and can thus study the interaction of the clumps in great detail.

Because we are constrained by the fact, that there has to be an integer number of clumps, each containing an integer number of SPH particles, we ended up with placing $128^2 = 16384$ baryonic clumps into the box, each with 128 baryonic particles and replacing 13 dark matter particles. This gives a baryonic fraction $f_b = 0.102$, very close to the desired value. The initial conditions with the clumps contain then $(1 - f_b) \cdot 128^3 = 1884160$ dark matter particles (with a mass of $m_{\text{DM}} = 4.0 \cdot 10^7 h^{-1} M_\odot$ for the $10h^{-1}$ Mpc box) and 128^3 SPH particles (with a mass of $m_b = 4.0 \cdot 10^6 h^{-1} M_\odot$). The mass and radius of a clump are $M_{\text{cl}} = 5.2 \cdot 10^8 h^{-1} M_\odot$ and $R_{\text{cl}} = 0.11h^{-1}$ Mpc, respectively, with an average separation of $d_{\text{cl}} = 0.39h^{-1}$ Mpc (all length scales given are in comoving coordinates). Our choice of clump mass is motivated by the desire to have $M_{\text{cl}} \ll M_{\text{fs}}$, but still large enough to be resolved in the simulations. Any other choice of M_{cl} would lead to very similar results, provided $M_{\text{cl}} \ll M_{\text{fs}}$ — see below.

The clumps are distributed irregularly throughout the simulation volume, with their centers forming a glass-like structure. The 13 closest dark matter particles to a clump center are removed, and the resulting void is filled with a

sphere containing 128 SPH particles, also with a glass-like distribution, which furthermore is oriented at random. This procedure assures that the initial density field is not disturbed, and that neighboring clumps do not overlap initially. (Random placement of the clump centers would result in many overlapping clumps as their average separation is not much larger than their size, $d_{\text{cl}} \approx 3.5R_{\text{cl}}$.)

For the control simulations with evenly distributed baryonic matter, one SPH per dark matter particle was added within one SPH softening length (Sommer-Larsen & Dolgov 2001) and with a mass f_b times the original dark matter particle mass. Since no dark matter particles were removed, their masses were reduced to $(1 - f_b)$ the original value. Thus m_b is the same as in the simulations with clumps, whereas now $m_{\text{DM}} = 3.6 \cdot 10^7 h^{-1} M_{\odot}$.

From these initial conditions, which now contain SPH particles, regions were cut out corresponding to the subvolumes, from which the galaxies of interest form in the pure dark matter simulation, as identified by tracing their particles back to the initial conditions. (Care is taken to make sure that no clumps are intersected by the region boundaries in simulations with baryonic clumps.) Only inside these areas are the gas particles included, whereas for the surrounding region the original pure dark matter initial conditions were used, with the dark matter particles increasingly coarsely resampled with increasing distance from the galaxy forming subvolume. That way, the formation of individual galaxies can be followed in detail within the correct cosmological setting, see e.g. Navarro & White (1994); Gelato & Sommer-Larsen (1999); Thacker & Couchman (2000); Sommer-Larsen, Götz & Portinari (2003).

Initially, the SPH particles are assigned a thermal energy corresponding to a temperature $T \approx 55$ K. Gravitational interactions are softened according to the prescription of Hernquist & Katz (1989). The softening lengths are $1.3h^{-1}$ kpc for gas and star particles, $2.9h^{-1}$ kpc for the dark matter particles inside the galaxy forming region in simulations with clumps, and $2.8h^{-1}$ kpc for such dark matter particles in runs with evenly distributed baryonic matter. The softening lengths of the dark matter particles in the coarsely resampled surrounding are correspondingly larger.

5.4 The Simulations

We selected two dark matter haloes (numbers 19 and 27) from the cosmological N-body simulation for further study with the TreeSPH code. The haloes have characteristic circular velocities comparable to or a little below that of the Milky Way. These galaxies were chosen according to the criteria laid out above, and because they show distinct disc-like morphologies and exponential surface density profiles in the TreeSPH-runs with evenly distributed baryonic matter. For each of the haloes, six simulations with different combinations of cooling function metallicity, star formation efficiency, and presence or absence of baryonic clumps, were run, as can be seen in Table 5.3. The simulations of the larger halo, #19, contain about 34000 dark matter and 22000 (without clumps) or 32000 (with clumps) SPH particles initially, whereas the runs for halo #27 consist of about 26000 dark matter and 14000 (without clumps) or 23000 (with clumps) gas particles at the start. The significantly

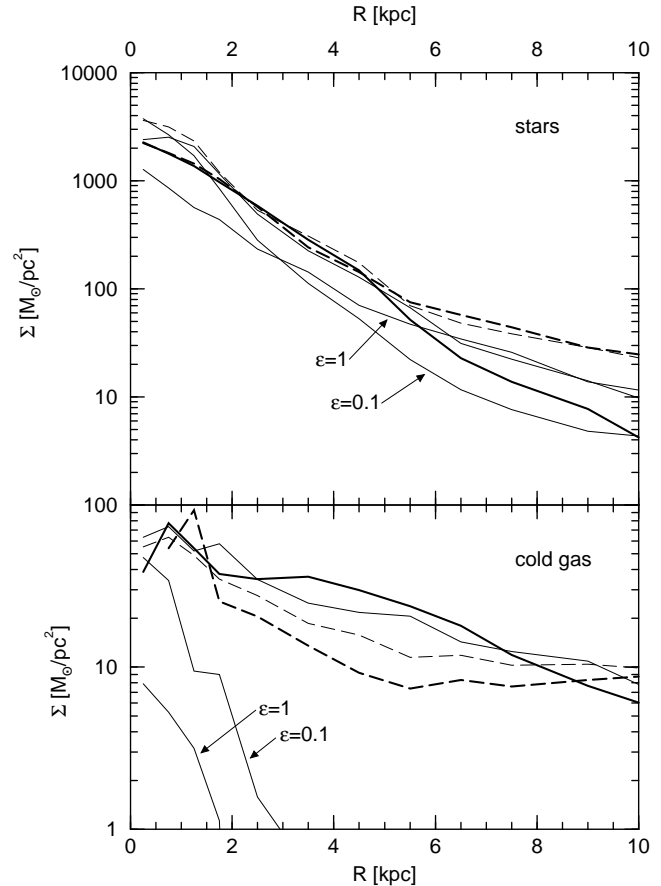


Figure 7. Surface density profiles for Milky Way like disc galaxy #19 in stars (top) and cold gas with $T < 3 \cdot 10^4$ K (bottom) at $z = 0$. Thick lines denote runs with evenly distributed baryonic matter, and thin lines those with baryonic clumps. Simulations with primordial abundance are shown as solid lines, and the 1/3 solar metallicity cases ($[\text{Fe}/\text{H}] = -0.5$) by dashed lines. The SFE is $\varepsilon = 0.01$, unless otherwise noted. The scale lengths for the stellar discs lie between 1 kpc and 1.5 kpc.

higher number of SPH particles in simulations with baryonic clumps is due to the fact that their initial regions have to be extended to avoid that clumps are intersected by the boundaries of the galaxy-forming subvolumes.

5.5 Results

5.5.1 Properties at $z = 0$

In all of the TreeSPH-simulations, the galaxies show clear disc-like morphologies and kinematics, with the bulk of the stars on approximately circular orbits in the disc. Most of the remaining stars are found in an inner, bulge-like component and finally a small fraction in a dynamically insignificant stellar halo surrounding the disc. The disc galaxies formed in our simulations are thus qualitatively very similar to observed disc galaxies, like the Milky Way, irrespective of the presence or absence of baryonic clumps initially, and of the assumed values for the IGM metallicity and SFE.

All of the discs have approximately exponential surface density profiles in stars and cold gas out to four scale lengths. As an example, the profiles for the different simulations

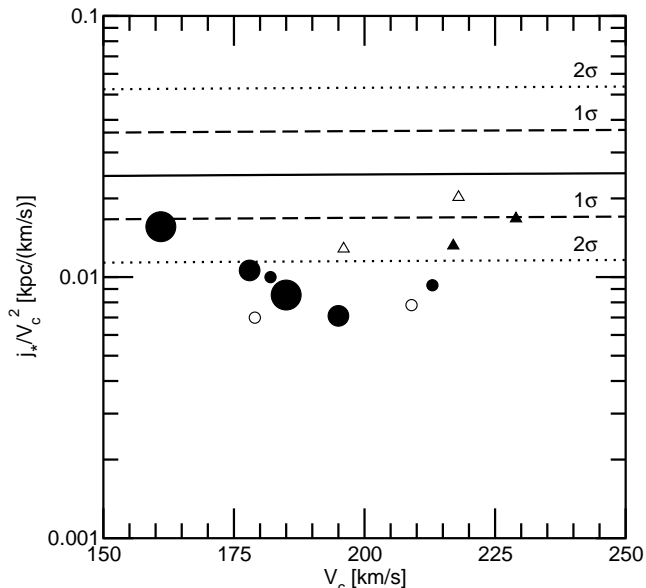


Figure 8. The normalized specific angular momenta in stars j_*/V_c^2 at $z = 0$ of the disc galaxies formed in the simulations. Small symbols are for runs with a SFE $\varepsilon = 0.01$, medium sized ones have $\varepsilon = 0.1$, and the large ones $\varepsilon = 1$. The round symbols denote primordial abundance, and the triangles a metallicity of $[\text{Fe}/\text{H}] = -0.5$. Open symbols are used for the control simulations with evenly distributed baryonic matter, whereas filled symbols are for runs with baryonic clumps. The solid line shows the median value from observational data on disc galaxies (Byun 1992), obtained as explained in Sommer-Larsen & Dolgov (2001), but using $H_0 = 65 \text{ km/s/Mpc}$, the dashed and dotted lines bracket the 1σ and 2σ intervals around the median.

of galaxy #19 are shown in Fig. 7. The exponential scale lengths for the stellar discs lie between 1 kpc and 1.5 kpc. The runs with 1/3 solar metallicity (dashed lines in Fig. 7) show somewhat flatter gas and stellar profiles and a lower density in cold gas, since the more effective cooling leads to a higher conversion rate of gas into stars. The simulations with a higher SFE (as marked in Fig. 7) have, as one would expect, much depleted gas discs, and lower surface densities in stars, since their star formation rates peak at higher redshifts (see below). Thus more stars are formed initially in the halo, and less gas is left to form the disc stars.

The scale lengths of the stellar discs (see Fig. 7) are somewhat low compared to observed values — thus the angular momentum problem has not been completely overcome. This can also be seen by looking at the normalized specific angular momenta in stars $\tilde{j}_* = j_*/V_c^2$ plotted in Fig. 8 for the two discs in all the different simulation runs. As argued by Sommer-Larsen, Gelato & Vedel (1999) one expects \tilde{j}_* to be almost independent of V_c on both theoretical and observational grounds. On average, the normalized specific angular momenta of our discs lie only about a factor of two below the median observed value, as obtained by Sommer-Larsen & Dolgov (2001). This compares well with other attempts to solve the angular-momentum problem, e.g. the WDM models of Sommer-Larsen & Dolgov (2001) and CDM scenarios with feedback (Sommer-Larsen, Götz & Portinari 2003), which

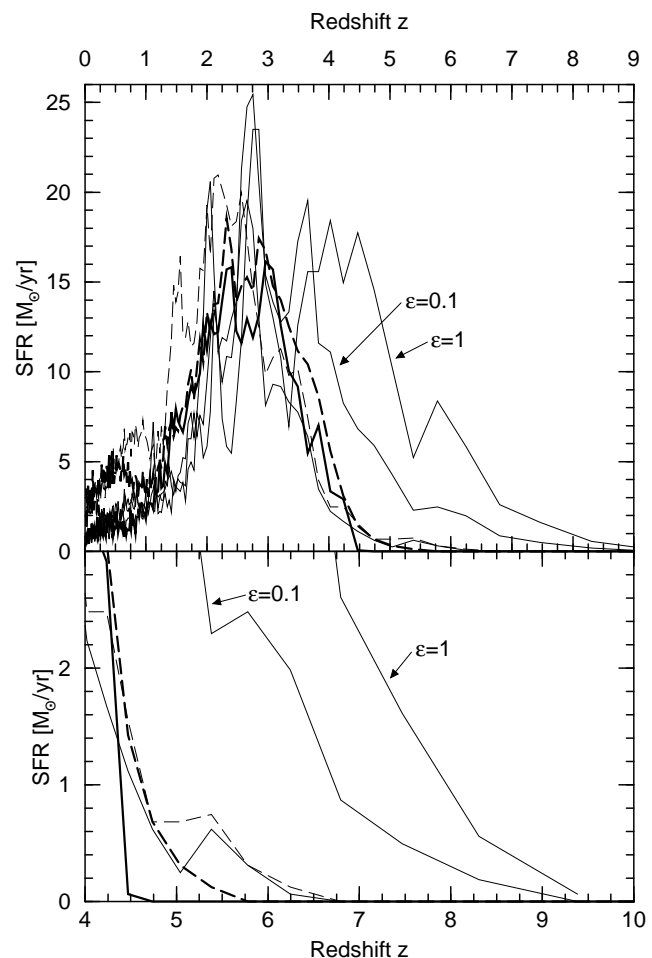


Figure 9. Star formation rates in M_\odot/yr for the different simulations of galaxy #19, with a magnification of the high-redshift tail at the bottom. Line styles are as in Fig. 7.

also come within a factor of two to three of the observed specific angular momenta.

In Table 5.3 and Figs. 7 and 8, we have included the results for the simulations with high SFE $\varepsilon = 0.1$ and $\varepsilon = 1$ at $z = 0$, even though these runs were initially carried out only to study the effect, a possible high SFE at large redshifts would have on early star formation. As expected, these simulations produce discs which have an unrealistically low cold gas fraction, indicating that the SFE can not stay constant at these large values. In spite of that, their specific angular momenta lie in the same range as that of the other runs (see Fig. 8), indicating that SFE is not an important parameter in WDM models with baryonic clumps for solving the angular momentum problem.

5.5.2 The High-Redshift Evolution

The present-day properties of disc galaxies are thus unaffected by the presence or absence of baryonic clumps. In both cases do we find discs at redshift $z = 0$ with the same kinds of profiles and specific angular momenta. The reason for this lies in the behavior of the clumps at the beginning of structure formation.

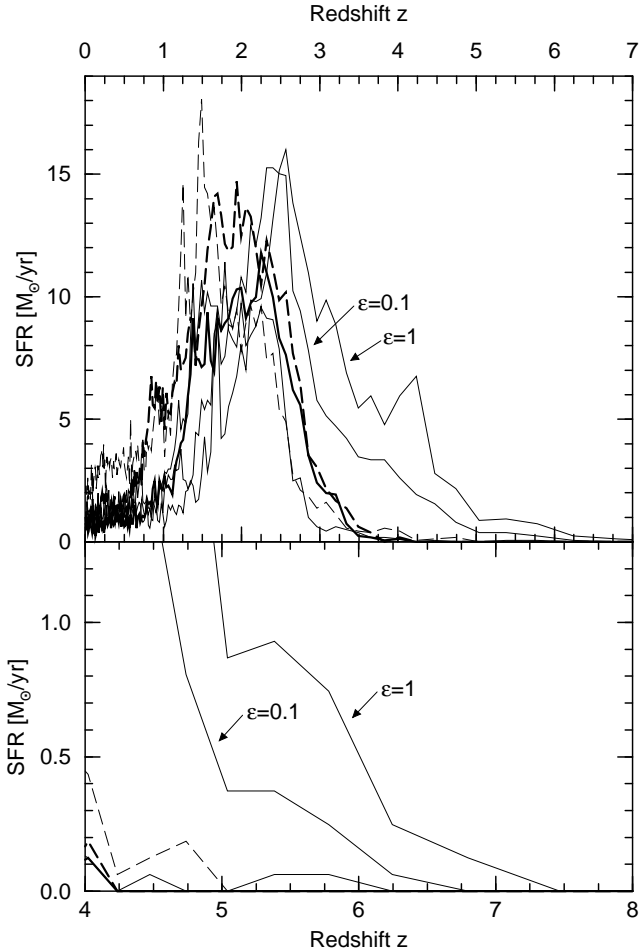


Figure 10. Same as Fig. 9, but now for galaxy #27.

When the first sheets and filaments form at high redshifts, the baryonic clumps get rapidly distorted into ellipsoidal shapes by the tidal field of these structures. The clumps get ‘gently’ incorporated into the filaments, and there are no shocks occurring during this, or when the clumps eventually physically touch. After 1.0–1.5 Gyr ($z=4$ –5), the filaments in the simulations with baryonic clumps are almost evenly filled with baryonic matter, after which the same processes of galaxy formation take place as in the ordinary WDM scenario with evenly distributed baryonic matter (The clumps do though survive much longer in the voids, but this is not of interest here, since the early galaxy/star formation in the simulations takes place in the filaments). During filament formation, also the dark matter becomes distributed smoothly in the filaments. This general behaviour strongly suggests that the main results of the simulations do not depend of the specific choice of clump mass, as previously mentioned.

But there is a significant difference between the clump and no-clump models in terms of the early star formation history. Figs. 9 and 10 show the star formation rates for the two selected galaxies in all the model runs. In the simulations with baryonic clumps, the first stars form earlier than in those without them. This is not surprising, since the baryonic matter in the models with clumps starts out with a

higher density. If one only applied a density criterion as the star formation recipe, one could get star formation started very early in WDMB. But the initial gravitational compression and deformation of the clumps heats the baryonic material, and afterwards a balance between Hubble expansion and tidal gravitational squeezing is achieved for some time, keeping the baryonic density in the clumps approximately constant. Only after turn-around has the baryonic material in the clumps a chance to cool efficiently and to start forming stars. This is why we have included the condition, that the gas velocity field needs to be compressive in star forming regions, into our star formation recipe.

The first stars form at an epoch $z_{*,i}$ which is of order a period t_* after the first region with a compressive gas velocity field and $n_H > n_{H,c}$ appears. For the standard WDM simulations with $\epsilon = 0.01$ $z_{*,i} \simeq 4.5$; cf. Figures 9 and 10 (the $[\text{Fe}/\text{H}]=-0.5$ cooling function simulations are clearly inappropriate when discussing the formation of the *first* stars). The similar WDMB simulations have $z_{*,i} \simeq 6.5$. The WDMB simulations with higher SFEs ($\epsilon = 0.1$ and 1) have $z_{*,i}=7$ –9.5. We did not run standard WDM simulations with $\epsilon = 0.1$ and 1, but based on the $\epsilon = 0.01$ simulations we estimate that even for such high SFEs $z_{*,i} \lesssim 5.5$. Hence going to the WDMB model brings the warm dark matter model in much better agreement with observations of high- z galaxies (e.g. Hu et al. 2002 — $z=6.56$) and QSOs (e.g. Fan et al. 2001 — several with $z > 6$). In fact for the high SFE simulations there is even marginal agreement with the value of the redshift of reionization of the Universe $z_{\text{re}} \gtrsim 10$ recently claimed by the WMAP team (Spergel et al. 2003), provided reionization happens shortly after the onset of star formation — but see below. We note that Sommer-Larsen, Götz & Portinari (2003) find that the SFE likely was considerably higher during the early phases of galaxy formation than at present. For $z \gtrsim 10$ the gas velocity field is everywhere expansive, so it will not be possible to push $z_{*,i}$ beyond ≈ 10 .

6 SUMMARY AND CONCLUSIONS

We have investigated the implications of strongly inhomogeneous, primordial baryon distribution on sub-galactic scales ($10M_\odot \ll M \ll 10^{11}M_\odot$) for Big Bang Nucleosynthesis, CMB anisotropies and galaxy formation in the context of the warm dark matter model. Big Bang Nucleosynthesis is only slightly changed relative to SBBN, but the change in recombination history at $z \sim 1500 - 700$ relative to “standard” theory leads to differences in the anisotropy and polarization power spectra, which should be detectable by the Planck satellite provided systematic effects can be understood. We show by fully cosmological, hydro/gravity simulations that the formation of galactic discs is only weakly affected by going from the WDM to the WDMB scenario. In particular, the final disc angular momenta (at $z=0$) are as large as for the standard case and the “disc angular momentum problem” is solved to within a factor of two or better without invoking (hypothetical) energetic feedback events. A very desirable difference from the standard WDM model, however, is that the on-set of star (and AGN) formation happens earlier. For the “optimal” free-streaming mass of $M_f \sim 1.5 \cdot 10^{11} h^{-1} M_\odot$ the redshift of formation of the first stars increases from $z_{*,i}=4$ –5 to $\gtrsim 6.5$, in much better

agreement with observational data on high-redshift galaxies and QSOs. The WDM model is, however, for this choice of free-streaming mass still limited to $z_{*,i} \lesssim 10$, so probing the “dark ages” with JWST, ALMA etc. will offer direct tests of this theory.

7 ACKNOWLEDGEMENTS

We have benefited from comments by M. Demianski, A. Doroshkevich, L. Portinari and M. Way. This project was supported by Danmarks Grundforskningsfond through its support for the establishment of the Theoretical Astrophysics Center.

REFERENCES

- Abramo L.R., Finelli F., 2001, *Phys. Rev. D*, 64, 083513
 Affeck I., Dine M., 1985, *Nucl. Phys. B*, 249, 361
 Balsara D.S., 1995, *J. Comp. Phys.*, 121, 357
 Bartolo N., Matarrese S., Riotto A., 2001, *Phys. Rev. D*, 64, 123504
 Bode, P., Ostriker, J.P., Turok, N., 2001, *ApJ*, 556, 93
 Bond, R. J., Crittenden, R., 2001, in Crittenden, R., Turok, N., eds., *Structure Formation in the Universe*. Kluwer, Dordrecht, p. 241
 Bryan G.L., 1999, *Computing in Science and Engineering*, 1:2, 46
 Bryan G.L., 2002, in preparation
 Bucher M., Moodley K., Turok N., 2001, *Phys. Rev. Lett.*, 87, 191301
 Byun Y.-I., 1992, PhD thesis, The Australian National University
 Carlberg, R.G., et al., 1996, *ApJ*, 462, 32
 Couchman H.M.P., Thomas P.A., Pearce F.R., 1995, *ApJ*, 452, 797
 de Bernardis P. et al., 2000, *Nature*, 404, 955
 Dolgov A., Silk J., 1993, *Phys. Rev. D*, 47, 2619
 Demianski, M., Doroshkevich A.G., 2003, *ApJ*, in press (astro-ph/0304484)
 Doroshkevich A.G., Naselsky I.P., Naselsky P.D., Novikov I.D., 2003, *ApJ*, 586, 709
 Doroshkevich, A., Zel’dovich, Ia. B., Novikov, I. D., 1967, *Sov. Astr.*, 11, 233
 Eke V.R., Cole S., Frenk C.S., 1996, *MNRAS*, 282, 263
 Ettori S., Fabian A.C., 1999, *MNRAS* 305, 834
 Fan, X., et al., 2001, *AJ*, 122, 2833
 Fukugita, M. Hogan, C.J., Peebles, P.J.E., 1998, *ApJ*, 518, 503
 Gelato S., Sommer-Larsen J., 1999, *MNRAS* 303, 321
 Gnedin, N.Iu., Ostriker, J.P., 1992, *ApJ*, 400, 1
 Götz M., Sommer-Larsen J., 2002, *Astroph. Sp. Sc.*, 281, 415
 Haardt F., Madau P., 1996, *ApJ*, 461, 20
 Hanany S. et al., 2000, *ApJ*, 545, L5
 Hernquist L., Katz N., 1989, *ApJS*, 70, 419
 Hogan, C., Loeb, A., 1993, *ApJ*, 415, 63
 Hu, E.M., et al., 2002, *ApJ*, 568, L75
 Jedamzik K., Rehm J.B., 2001, *Phys. Rev. D*, 64, 023510
 Klypin, A., Kravtsov, A. V., Valenzuela, O., Prada, F., 1999, *ApJ*, 523, 32
 Leitch, E.M., et al., 2002, *Nature*, 410, 763L
 Lesgourgues, J., Peloso, M., 2000, *Phys. Rev. D*, 62, 081301
 Liu G.-C., Yamamoto K., Sygyiyama N., Nishioka H., 2001, *ApJ*, 547, 1
 Malaney R.A., Butler M.N., 1989, *Phys. Rev. Lett.*, 62, 117
 Mason, B.S., et al., 2003, *ApJ*, 591, 540
 Monaghan J.J., Gingold R.A., 1983, *J. Comp. Phys.*, 52, 374
 Moore, B., et al., 1999a, *ApJ*, 524, L19
 Moore, B., et al., 1999b, *MNRAS*, 310, 1147
 Naselsky P.D., Novikov I.D., 2002, *MNRAS*, 334, 137
 Navarro J.F., Benz W., 1991, *ApJ*, 380, 320
 Navarro J.F., Frenk C.S., White S.D.M., 1995, *MNRAS*, 275, 56
 Navarro J.F., Steinmetz M., 1997, *ApJ*, 478, 13
 Navarro J.F., White S.D.M., 1994, *MNRAS*, 267, 401
 Novikov D.I., Schmalzing J., Mukhanov V.F., 2000, *A&A*, 364, 17
 Olive K.A., Steigman G., Walker T.P., 2000, *ApJ*, 333, 389
 Peebles, P.J.E., 1967, *ApJ*, 147, 859
 Peebles, P.J.E., 2001, *ApJ*, 557, 495
 Peebles, P.J.E., Juszkewich, R., 1998, *ApJ*, 509, 483
 Peebles P.J.E., Seager S., Hu W., 2000, *ApJ*, 539, L1
 Polarski D., Starobinsky A., 1994, *Phys. Rev. D*, 50, 6123
 Riazuelo A., Langlos D., 2000, *Phys. Rev. D*, 62, 043504
 Seager S., Sasselov D.D., Scott D., 2000, *ApJS*, 128, 407
 Seljak U., Zaldarriaga M., 1996, *ApJ*, 469, 437
 Silk J., 1997, *ApJ*, 481, 703
 Sommer-Larsen J., Dolgov A., 2001, *ApJ*, 551, 608
 Sommer-Larsen J., Gelato S., Vedel H., 1999, *ApJ*, 519, 501
 Sommer-Larsen J., Götz M., Portinari L., 2003, *ApJ*, in press (astro-ph/0204366)
 Spergel, D. N., et al., 2003, *ApJ*, in press (astro-ph/0302209)
 Sutherland R.S., Dopita M.A., 1993, *ApJS*, 88, 253
 Tegmark, M., Zaldarriaga, M., 2000, *Phys. Rev. Lett.*, 85, 2240
 Thacker R.J., Couchman H.M.P., 2000, *ApJ*, 545, 728
 Vedel H., Hellsten U., Sommer-Larsen J., 1994, *MNRAS*, 271, 743
 White S.D.M., 1996, in R. Schaeffer et al. (eds.), *Cosmology and Large-Scale Structure: Les Houches, Session LX*, Elsevier, Amsterdam, p. 349
 White, M., Scott, D., Pierpaoli, E., 2000, *ApJ*, 545, 1
 Yokoyama J., Sato Y., 1991, *ApJ*, 379, 427
 Zeldovich, Ia. B., Novikov, I. D., 1983, *Relativistic Astrophysics Vol.2*, University of Chicago Press, Chicago, IL